

Dalton Transactions

Accepted Manuscript



This article can be cited before page numbers have been issued, to do this please use: Y. Li, B. Jia, Q. Liu, M. Cai, Z. Xue, Y. Fan, H. Wang, C. Su and G. Li, *Dalton Trans.*, 2018, DOI: 10.1039/C8DT02706D.



This is an Accepted Manuscript, which has been through the Royal Society of Chemistry peer review process and has been accepted for publication.

Accepted Manuscripts are published online shortly after acceptance, before technical editing, formatting and proof reading. Using this free service, authors can make their results available to the community, in citable form, before we publish the edited article. We will replace this Accepted Manuscript with the edited and formatted Advance Article as soon as it is available.

You can find more information about Accepted Manuscripts in the [author guidelines](#).

Please note that technical editing may introduce minor changes to the text and/or graphics, which may alter content. The journal's standard [Terms & Conditions](#) and the ethical guidelines, outlined in our [author and reviewer resource centre](#), still apply. In no event shall the Royal Society of Chemistry be held responsible for any errors or omissions in this Accepted Manuscript or any consequences arising from the use of any information it contains.



Journal Name

ARTICLE

MOFs-derived Mn doped porous CoP nanosheets as efficient and stable bifunctional electrocatalysts for water splitting

Yinle Li,‡ Baoming Jia,‡ Qinglin Liu, Mengke Cai, Ziqian Xue, Yanan Fan, Hai-Ping Wang, Cheng-Yong Su, Guangqin Li*

Received 00th January 20xx,
Accepted 00th January 20xx

DOI: 10.1039/x0xx00000x

www.rsc.org/

Searching for the highly active and stable bifunctional electrocatalysts for overall water splitting, e.g., for both of hydrogen evolution reaction (HER) and oxygen evolution reaction (OER), is dominating in terms of operating future renewable energy storage and conversion processes to reality. In this work, a kind of two-dimensional ultrathin manganese (Mn) doped polyhedral cobalt phosphide (Mn-CoP) have been synthesized with the etching-carbonization-phosphidation of Co-centered metal-organic frameworks. The as-prepared porous Mn-CoP nanosheets have larger specific surface area and higher porosity furnishing more plentiful catalytic active sites than its counterpart hollow CoP and Mn-CoP nanoparticles, thus show much better electrocatalytic activity for both HER and OER in acidic and alkaline media. In addition, the Mn-CoP nanosheets also demonstrate excellent durability after long-term operations. The high performances are attributed to the synergistic effects of CoP nanosheets with intrinsic activity, graphitic carbon and controllable electronic structure doped by Mn and N elements. This synthetic methodology of using a classical MOF as a precursor to build a new 2D sheet-like composite may create the opportunities to search highly efficient and robust non-precious metal catalysts for energy-related reactions.

Introduction

Hydrogen, as a green energy with high energy density, has attracted much attention because its combustion products do not contain carbon dioxide during the energy conversion process.¹ Hydrogen evolution reaction (HER) is an efficient and reliable technology for hydrogen production with a simple process, low pollution, and high-grade product purity.² However, the high cathodic overpotential result in the increasing electrolysis cell voltage and large power consumption, which directly limited it large-scale industrial application.³ On the contrary, oxygen evolution reaction (OER) is also a critical step in various types of renewable-energy conversion techniques, such as water splitting for hydrogen evolution and rechargeable metal-air batteries.⁴ Nevertheless, the multiple proton-couple electron transfer steps for OER leads to intrinsically sluggish reaction kinetics.⁵ As the benchmarking HER and OER electrocatalysts, Pt and RuO₂ suffer from limited reserves and high cost, severely hampering their wide applications.⁶ Therefore, synthesis of stable, active, non-noble metal-based electrocatalysts for both HER and OER of water splitting has been a long-standing challenge.⁷

Up to date, a wide variety of nanomaterials have been immensely

explored (e.g., transition metal sulfides, nitrides and phosphides) for the purpose of reducing the energy consumption of water splitting.⁸⁻¹² Particularly, the transition metal phosphides (TMPs) are a representative class of metalloid compounds with outstanding HER performance because of their similarity with hydrogenase, which act as a hopeful candidate for water splitting.¹³⁻¹⁸ However, TMPs still suffer from relatively high overpotential and sluggish reaction kinetics; besides, their OER activity are rarely demonstrated, which deteriorates their catalytic property for overall water splitting.¹⁹⁻²⁰ Therefore, to maximize the catalytic performance of TMP-based nanomaterials via exposing more catalytically active sites is highly desirable and remains a big challenge. Previous studies demonstrated that the catalytic efficiency of TMPs can be enhanced through the hybridization with nanocarbon materials and doping of heteroatoms (such as Ni,²¹ Al,²² Mn,²³ Mo,²⁴ Cu²⁵). Zeolitic imidazolate frameworks (ZIFs), especially ZIF-67 and ZIF-8, are a kind of classical porous materials with zeolite-like structures.²⁶ The abundant carbon, nitrogen-containing ligands and high metal contents are anticipated to be good precursor and template to design various fascinating metal-carbon or metal-nitrogen hybrid nanomaterials and the corresponding TMPs derivatives.²⁷⁻³² Furthermore, among various nanostructures, ultrathin nanosheets demonstrated well-defined planar structures and a large surface area, which are advantage for charge transfer and mass transport in electrocatalysis.³³ However, until now, the design of novel TMPs nanosheets structures doped with heteroatoms as capable bifunctional HER and OER catalysts is still a big challenging task and rarely reported.

MOE Laboratory of Bioinorganic and Synthetic Chemistry, Lehn Institute of Functional Materials, School of Chemistry, Sun Yat-Sen University, Guangzhou 510275, P. R. China; E-mail: liguangqin@mail.sysu.edu.cn

† Footnotes relating to the title and/or authors should appear here.

Electronic Supplementary Information (ESI) available: additional structural characterizations. See DOI: 10.1039/x0xx00000x

‡ these authors contributed equally to this work

Here, we report a novel hybrid nanostructure composed of CoP nanosheets doped with Mn element (Mn-CoP) through an etching-carbonization-phosphidation strategy derived from rhombic dodecahedral ZIF-67 particle. The Mn-CoP nanosheets reveal remarkable electrocatalytic activity for HER, with the onset overpotentials of 75 and 110 mV, Tafel slopes of 61 and 85 mV dec⁻¹, and overpotentials of 148 and 195 mV to reach 10 mA cm⁻² in acidic 0.5 M H₂SO₄ and alkaline 1 M KOH media, respectively, which are observably superior to those of hollow CoP, Mn-CoP nanoparticles. Observably, the overpotentials of 290 mV to reach 10 mA cm⁻² for OER performance comparable to that of commercial RuO₂ catalysts. Importantly, both the HER and OER demonstrated excellent stability after uninterrupted working for 20 h and 30 h, respectively. The flexible synthesis procedure of heteroatom doping TMDs nanosheets offers a promising strategy to develop low-cost electrocatalysts with remarkable catalytic activity and excellent stability for electrochemical overall water splitting.

Experimental

Synthesis of ZIF-67: All the chemicals were used without further purification. In a typical synthesis, 1455 mg Co(NO₃)₂·6H₂O was dissolved in 100 mL methanol as solution A, and 3284 mg 2-methylimidazole was dissolved in 100 mL methanol as solution B. Then, solution A was poured slowly into the solution B under magnetic stirring. After 1 hour, the mixed solution was aged for 24 h. The obtained purple product was collected by centrifugation and dried at 60 °C for 12 h. The diameter of the ZIF-67 was about 300 nm.

Synthesis of CoO polyhedral: The abovementioned ZIF-67 was placed in a tube furnace under Ar atmosphere at 450 °C for 2 h with a ramping rate of 2 °C·min⁻¹. The products were obtained when the system was cooled to room temperature.

Synthesis of ultrathin porous MnCo₂O₄ nanosheets: 120 mg ZIF-67 was dispersed in 20 mL ethanol with sonication. Then, 343.88 mg Mn(NO₃)₂·4H₂O was dissolved in 10 mL deionized water and mixed with ZIF-67 solution. The mixed solution was refluxed at 85 °C for 10 minutes. The colour of the solution first turned blue and gradually evolved into pink, finally dark brown. The ultrathin porous MnCo₂O₄ nanosheets were obtained by centrifugation and washed with ethanol. In order to improve the graphitization and conductivity of the product, the ultrathin porous MnCo₂O₄ nanosheets were placed in a tube furnace under Ar atmosphere at 450 °C for 2 h with a ramping rate of 2 °C·min⁻¹.

Synthesis of MnCo₂O₄ nanocrystals: MnCo₂O₄ nanocrystals were prepared according to previous literature. 700 mg of Co(NO₃)₂·6H₂O and 200 mg of MnSO₄·H₂O were dissolved in 55 mL of deionized water. Subsequently, 5 mL of 1.44 M NaOH aqueous solution was added dropwise into the reaction mixture under vigorous stirring. After magnetic stirring for 30 min, the above solution was transferred into a 100 mL Teflon-lined stainless-steel autoclave. The hydrothermal reaction was carried out at 160 °C for 10 h. The product was collected by centrifugation and washed with water and ethanol. Finally, the dried powder was calcined in N₂ at 600 °C for 2 h with a ramping rate of 2 °C·min⁻¹.

Synthesis of ultrathin porous Mn-CoP nanosheets: 20 mg of ultrathin porous MnCo₂O₄ nanosheets were put in a tube furnace,

and 400 mg of Na₂PH₂O₂·2H₂O was placed at the upstream side. The temperature of the furnace was elevated to 350 °C with a ramping rate of 2 °C·min⁻¹ and maintained for 2 h. The final products were obtained when the system was cooled to room temperature. Mn-CoP nanocrystals and CoP polyhedral were synthesized with the same procedure except the precursor was MnCo₂O₄ nanocrystals and CoO polyhedral.

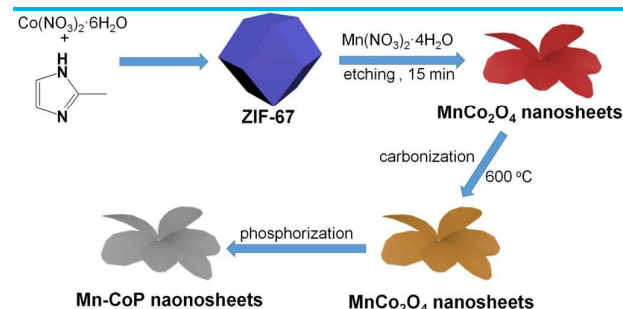
Characterizations: The morphology and structure were characterized by field-emission scanning electron microscopy (FESEM; Hitachi SU8010, 5 kV), transmission electron microscopy (TEM; JEOL, JEM-1400, 120 kV), Spherical aberration correction electron microscope (JEOL, ARM200, 300kV), Powder X-ray diffraction (XRD) patterns were recorded on a MiniFlex 600 (Rigaku Co., Japan) diffractometer with Cu Kα (λ = 1.5418 Å) radiation. The N₂ adsorption-desorption isotherms were collected using a Micromeritics Instruments 3Flex at 77 K. The surface properties of the products were analysed with X-ray photoelectron spectroscopy (XPS; VG ESCALABMKII instrument) with a Mg Kα X-ray source.

Electrochemical measurements: All the electrochemical measurements were implemented on a CHI 760E electrochemical workstation (CH Instruments, Inc., Shanghai) through a standard three-electrode system. A glassy carbon electrode (3 mm in diameter) was used as the working electrode. 5 mg of the catalysts and 20 μL Nafion solution were dispersed in 800 μL ethanol and 180 μL water, which was sonicated for 45 min to form ink. Then, 7 μL of the mixture ink was dripped onto the surface of glassy carbon electrode and dried at room temperature. The Ag/AgCl electrode in 3 M KCl solution and platinum wire were used as the reference electrode and counter electrode, respectively. The HER performance was evaluated in 0.5 M H₂SO₄ and 1 M KOH solutions, respectively. The OER performance was evaluated in 1 M KOH solution. The samples were evaluated by obtaining the polarization curves via linear sweep voltammetry (LSV) used a scan rate of 5 mV·s⁻¹. Electrochemical impedance spectroscopy (EIS) measurements were carried out at different potentials from 10⁵ to 0.1 Hz. The stability tests were performed by the cyclic voltammetry scanning 1000 cycles (CV, 100 mV·s⁻¹) for HER and 2000 cycles (CV, 100 mV·s⁻¹) for OER and also the long-term chronoamperometry. CV tests were also used to define the electrochemical double-layer capacitances (Cdl). The electrochemically active surface area could be assessed from the plot slope of the charging current vs. the scan rate. All the polarization curves in this work were carried out with IR compensation and converted to reverse hydrogen electrode (RHE).

Results and discussion

Scheme 1 illustrates the design strategy for the synthesis process of the Mn-CoP nanosheets. In a typical synthesis, three steps of etching-carbonization-phosphidation process were involved. ZIF-67 was fabricated as a sacrificial template through a simple one-pot reaction at room temperature, which was demonstrated by X-ray diffraction (XRD) (Figure S1a) and the Brunauer-Emmett-Teller (BET) surface area is 1225 m²·g⁻¹ (Figure S1b). Scanning electron microscopy (SEM) (Figure S1c-S1d) images illustrated that ZIF-67 showed well-defined rhombic dodecahedral with uniform size distributions and smooth surfaces. In the first step, a refluxing

process was performed in a mixed ethanol and water solution with the hard templates of rhombic dodecahedral ZIF-67 particle and etching agent of $\text{Mn}(\text{NO}_3)_2 \cdot 4\text{H}_2\text{O}$.



Scheme 1. Schematic illustration of the Synthesis Process of Mn-CoP Nanosheets

The phase and composition of obtained materials changing with the etching time. From the XRD patterns of different etching time (Figure S2), we can find that the product is mainly two-dimensional MnCo layered double hydroxide (MnCo-LDH) during a period of 10 min and then completely transform into two-dimension MnCo_2O_4 nanosheets after 15 min. The scanning electron microscopy (SEM) was carried out to explore the etching evolution process. After etching 5 min, parts of ZIF-67 transformed into nanosheets or hollow nanocages from the SEM of Figure S3a-S3c, but some of them kept the well-defined rhombic dodecahedral. After reaction with $\text{Mn}(\text{NO}_3)_2$ in mixture solvent for 10 min, the diffraction peaks of ZIF-67 particles are weaker in the XRD pattern (Figure S2) and the emerging (003), (006), and (009) peaks are unambiguously resulting from a typical LDH structure. This result strongly accounts for the successful formation of MnCo-LDH with the two-dimensional nanoplates structures, which was further illustrated by the SEM images (Figure S3d-S3f). During this process, the hydrolysis of Mn^{2+} ions can generate protons, which can gradually etch ZIF-67 particles and the released Co^{2+} ions can be partially oxidized forming into Co^{3+} ions by dissolved O_2 and NO_3^- ions. Then, the $\text{Co}^{2+}/\text{Co}^{3+}$ ions can coprecipitate with Mn^{2+} ions to produce MnCo-LDH nanosheets. Interestingly, the intermediate MnCo-LDH nanosheets totally transform into MnCo_2O_4 nanosheets after prolonging the etching time to 15 min, which demonstrated by the XRD pattern (Figure S2), and the SEM and transmission electron microscopy (TEM) images reveal that the morphology of MnCo_2O_4 nanosheets are similar to the MnCo-LDH nanosheets (Figure S3g-S3i, Figure S4). However, a large number of MnCo_2O_4 nanoparticles loaded on the surface of MnCo_2O_4 nanosheets after etching 20 min (Figure S3j-S3l), suggesting that the MnCo_2O_4 reunited under the high temperature.

In order to enhance the electric conductivity and nitrogen doping of MnCo_2O_4 nanosheets, the high-heat treatment was carried out in N_2 at 600 °C for 2 h. The destination product of two-dimension Mn-CoP nanosheets was further obtained from MnCo_2O_4 nanosheets by phosphorization calcination. The absence diffraction peaks of the MnCo_2O_4 phase can be completely replaced by the CoP phase (Figure 1a), which are assigned to the (011), (111), (112), (211), (103) and (020) planes of CoP (JCPDS 29-0497), respectively.

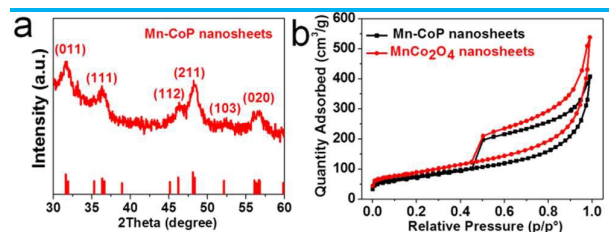


Figure 1 (a) XRD patterns of Mn-CoP nanosheets; (b) N_2 adsorption-desorption isotherm of the MnCo_2O_4 and Mn-CoP nanosheets

The pore structure information on the MnCo_2O_4 and Mn-CoP nanosheets catalyst was further characterized by N_2 sorption. As shown in Figure 1b, the typical type IV adsorption-desorption isotherm with an obvious hysteresis loop were observed for both the MnCo_2O_4 and Mn-CoP nanosheets, indicating plentiful mesoporous structure. Significantly, both the MnCo_2O_4 and Mn-CoP nanosheets show a large BET surface area of $412.5 \text{ m}^2 \cdot \text{g}^{-1}$ and $357.7 \text{ m}^2 \cdot \text{g}^{-1}$ with the pore volume of 1.15 and $1.04 \text{ cm}^3 \cdot \text{g}^{-1}$, respectively. Moreover, the pore size distribution curves (Figure S5) demonstrate that both the nanosheets show hierarchical pore structure with the pore size distribution of 2-15 nm. The porosity structure of the Mn-CoP nanosheets is advantageous for charge transfer efficiency and mass transport for electrocatalysis.³⁴

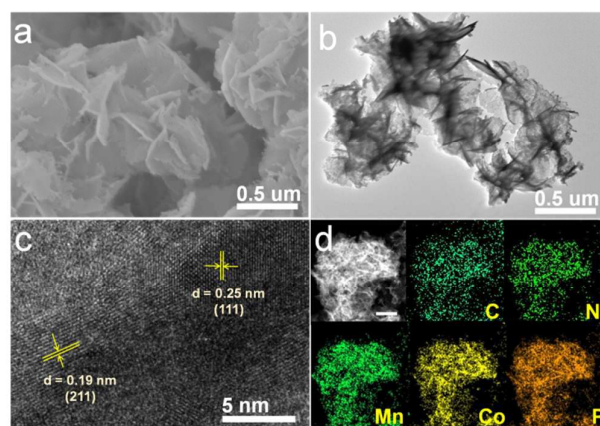


Figure 2 (a) SEM image of Mn-CoP nanosheets; (c and d) TEM and HR-TEM images of Mn-CoP nanosheets; (d) HAADF-STEM image of Mn-CoP nanosheets and elemental mapping of C, N, Mn, Co, P. (the bar in figure f is 300 nm)

To study the morphology of the obtained materials, SEM images of phosphatized product were shown in Figure 2a, fortunately, the Mn-CoP still remains the original nanosheets morphology, which can also be observed from TEM image in Figure 2b. The HRTEM image of the Mn-CoP nanosheets (Figure 2c) displayed the fringe spacing of 0.19 and 0.25 nm, which can be assigned to the CoP (211) and (111) lattice planes, respectively. The HAADF-STEM (Figure 2d) and corresponding EDS mapping also indicate that C, N, Mn, Co, and P elements were uniformly distributed on the Mn-CoP nanosheets. For comparison, the counterpart CoP and Mn-CoP nanoparticles were prepared by phosphorization calcination of CoO polyhedral and MnCo_2O_4 nanoparticles. After oxidization and

phosphorization calcination of precursor ZIF-67, the obtained CoP showed hollow structure with a surface area of $95.7 \text{ m}^2/\text{g}$ (Figure S6). The crystallinity, BET surface area and morphology structure of obtained Mn-CoP nanoparticles were also confirmed by XRD (Figure S7a), N_2 sorption ($39.7 \text{ m}^2/\text{g}$) (Figure S7b), SEM and TEM (Figure S7c and S7d). Compared to the nanosheets, Mn-CoP nanoparticles possess the lower BET surface area and irregular morphology, which may suggest the inferior electrochemical property of Mn-CoP nanoparticles since unfavourable charge transfer and mass transport.

The electrocatalytic HER activity of Mn-CoP nanosheets catalyst was first investigated in acidic $0.5 \text{ M H}_2\text{SO}_4$ and alkaline 1 M KOH with a standard three-electrode system. For comparison, a series of reference catalysts, including hollow CoP, Mn-CoP nanoparticles and commercial Pt/C, were also carried out. **Figure 3a and 3d** reveal the linear sweep voltammetry (LSV) curves of Mn-CoP nanosheets, hollow CoP and 20% Pt/C with a scan rate of $5 \text{ mV}\cdot\text{s}^{-1}$ under room temperature. As an anticipative, the 20% Pt/C catalyst presents the best HER activity. At the current density of $10 \text{ mA}\cdot\text{cm}^{-2}$, the Mn-CoP nanosheets catalyst shows superior catalytic performance with

lower overpotentials of 148 and 195 mV for HER than hollow CoP (310 and 355 mV) and Mn-CoP nanoparticles (305 and 522 mV, Figure S8) in acidic $0.5 \text{ M H}_2\text{SO}_4$ and alkaline 1 M KOH , respectively. The relevant Tafel slopes of the Mn-CoP nanosheets catalyst (61 and $85 \text{ mV}\cdot\text{dec}^{-1}$) are also smaller than those of hollow CoP (235 and $145 \text{ mV}\cdot\text{dec}^{-1}$) in acidic $0.5 \text{ M H}_2\text{SO}_4$ and alkaline 1 M KOH , respectively (**Figure 3b and 3e**), illustrating more beneficial electrocatalytic kinetics on the Mn-CoP nanosheets catalyst for the HER. The Tafel slope of the Mn-CoP nanosheets catalyst also demonstrates that the HER process is a Volmer-Heyrovsky pathway. The HER catalytic performance of current Mn-CoP nanosheets catalyst is also superior to many other reported catalysts (Tables S1 and S2). In addition, the Nyquist plots (Figure S9) also suggest that the Mn-CoP nanosheets catalyst has a smaller semicircle diameter compared with the counterpart CoP and Mn-CoP nanoparticles catalysts, proposing an advantageous charge transfer resistance (R_{ct}) for the Mn-CoP nanosheets catalyst in both acidic (-0.15 V , $R_{ct} = 30.25 \Omega$) and alkaline (-0.20 , $R_{ct} = 35.77 \Omega$) system.

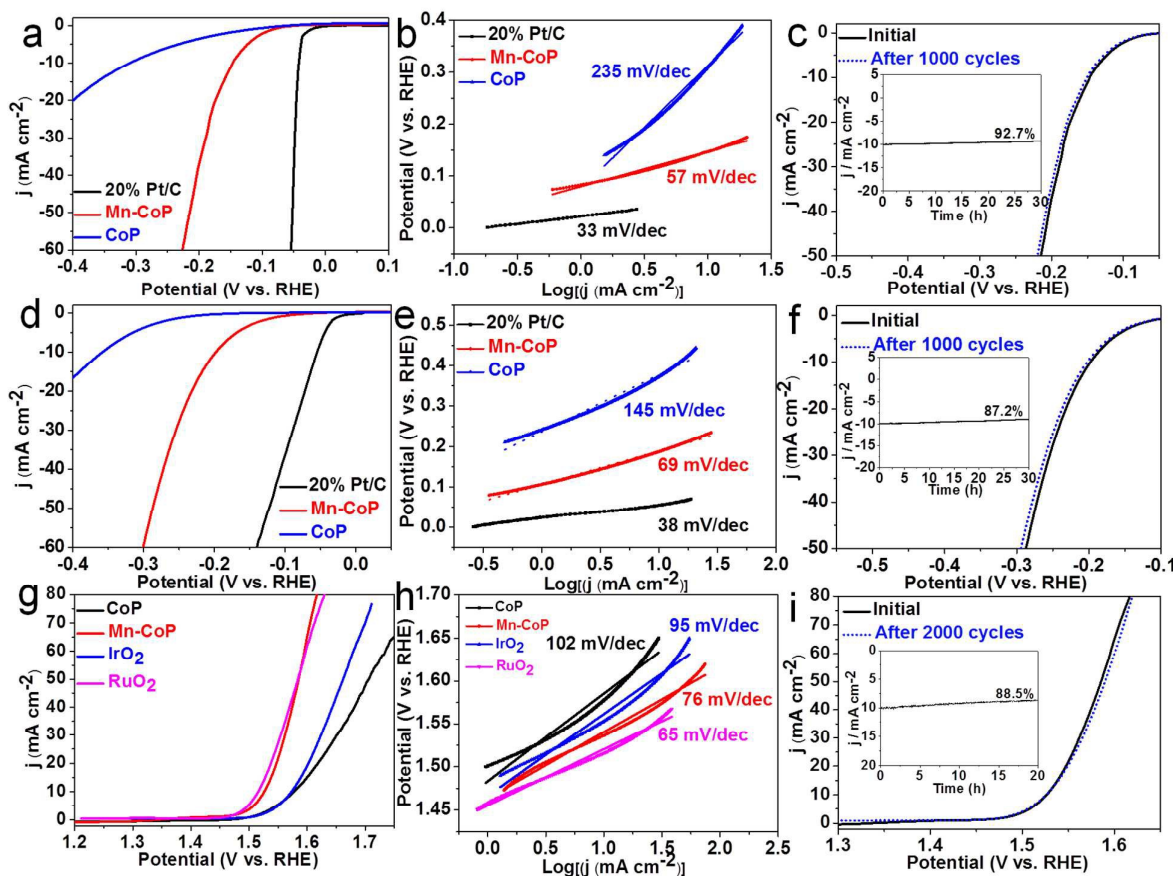


Figure 3. (a, b) LSV and Tafel curves of hollow CoP, Mn-CoP nanosheets and the compared Pt/C samples in $0.5 \text{ M H}_2\text{SO}_4$; (c) LSV curves of the Mn-CoP nanosheets catalyst before and after 1000 CV cycles for HER, the inset in (c) show the time-dependent current density curves with the Mn-CoP nanosheets catalyst; (d, e) LSV and Tafel curves 1 M KOH for HER; (f) the stability tset; (g, h) LSV and Tafel curves 1 M KOH for OER; (i) the stability tset.

To further study the catalytic activity, we evaluated the electrochemical active surface area (ECSA) by calculating the double-layer capacitances (Cdl), which can be acquired by cyclic voltammetry (CV) potential window with regular scan rates from 40 to 160 mV·s⁻¹ in a non-faradic potential district (Figure S10) in 1 M KOH. The Cdl of the Mn-CoP nanosheets catalyst (21.1 mF·cm⁻²) is superior to the CoP (12.2 mF·cm⁻²) and Mn-CoP nanoparticles catalyst (11.3 mF·cm⁻²) (Figure S10d), which implies that the Mn-CoP nanosheets catalyst has a larger ECSA, suggesting the better electrocatalytic performance for the HER. Furthermore, the stability of the Mn-CoP nanosheets catalyst was evaluated by scanning one thousand of CV cycles and long-term chronoamperometry. As shown in Figure 3c,f, comparing with the initial LSV curves, a negligible decay can be observed after 1000 cycles. Additionally, the time-dependent current-time curves (insets of Figure 3c,f) show that the catalytic performance of the Mn-CoP nanosheets catalyst could be sustained for at least 30 h in both acidic 0.5 M H₂SO₄ and alkaline 1 M KOH, respectively. Significantly, SEM, TEM, and HAADF-EDS mapping images suggest that the two-dimensional nanoplate morphology and the element composition of Mn-CoP nanosheets catalyst were maintained after long-term electrolysis (Figure S11). The XRD was also carried out to characterize the stability of crystalline structure after the cycles test (Figure S12). Significantly, the Mn-CoP nanosheets can maintain the diffraction pattern after 2000 cycles test.

The OER catalytic activity of the Mn-CoP nanosheets catalyst was further evaluated in 1 M KOH solution. Hollow CoP, Mn-CoP nanoparticles and commercial noble metal RuO₂ and IrO₂ were also assessed for comparison. Figure 3g is the LSV curves of all the catalysts with a scan rate of 5 mV·s⁻¹. The Mn-CoP nanosheets catalyst possessed the overpotential of 290 mV is lower than those of hollow CoP (342 mV), Mn-CoP nanoparticles (356 mV, Figure S13), and commercial IrO₂ (337 mV) at the current density of 10 mA·cm⁻², exhibiting the superior catalytic performance. Moreover, the corresponding Tafel slope (Figure 3h) of these samples also reveal the smallest Tafel value (76 mV·dec⁻¹) of Mn-CoP nanosheets compared with CoP (102 mV·dec⁻¹) and IrO₂ (95 mV·dec⁻¹), indicating higher OER activity of the Mn-CoP nanosheets catalyst. The Nyquist plots (Figure S14) also illustrate that the Mn-CoP nanosheets catalyst (1.55 V, Rct = 20.17 Ω) showed smaller charge-transfer resistance than the CoP catalyst (1.55 V, Rct = 58.6 Ω), due to the positive effect of Mn doping contributed to charge efficiency in electrocatalysis. Thus, Mn-CoP nanosheets catalyst was actually an outstanding catalyst and surpasses most of the reported non-noble-metal Co-based electrocatalysts for the OER in alkaline 1 M KOH media (Table S3). The stability of the Mn-CoP nanosheets catalyst was further carried out in 1 M KOH solution by CV scanning two thousand cycles and long-term chronoamperometry (Figure 3i). The LSV curve shows a negligible loss after 2000 cycles, and the OER activity can be continued for at least 20 h.

To understand the mechanism of Mn-CoP nanosheets for efficient bifunctional water splitting, the electronic states of Mn, Co, P and doping N of Mn-CoP nanosheets were investigated by X-ray photoelectron spectroscopy (XPS, Figure 4 and Figure S15). The XPS spectrum of Mn 2p region (Fig. 4a) shows two peaks located at 642 and 653 eV assigned to the binding energy (BE) of Mn 2p_{3/2} and Mn 2p_{1/2}, respectively. The peaks at 644.5 and 654.9 eV are

characteristic peaks of Mn⁴⁺, and the peaks of 641.7 and 653.2 eV are ascribed to Mn²⁺. As shown in Figure 4b, the XPS of Co 2p ranging from 793.0 to 805.0 eV and from 778.0 to 788.0 eV could be attributable to Co 2p_{1/2} and Co 2p_{3/2}, respectively. The obvious peaks for Co 2p_{3/2} at 778.6 and 794.1 eV is considered to the BE of Co in CoP, and the peaks at 782.2 and 797.1 eV accounting for the Co²⁺. The P 2p spectrum (Figure 4c) shows two peaks at 129.2 and 130.4 eV assigned to P 2p_{3/2} and P 2p_{1/2}, respectively. In addition, the broader peak at 134.0 eV could be attributable to PO_x or P-O species because of surface oxidation. Significantly, 129.2 eV of P 2p_{3/2} are considered to the standard binding energies of Co-P bond in CoP. Obviously, the XPS peaks of Co and P are positively and negatively shifted compared with the BE of metallic Co (778.1 eV) and P (130.2 eV), suggesting that the Co atom and P atom in CoP have a partial positive charge and negative charge, respectively. Therefore, the electron should transfer should from Co to P, which will facilitate adsorption and desorption of micromolecule reactant and product in the electrocatalysis process.³⁵⁻³⁸ The high-resolution N 1s spectrum reveals the presence of three types of N species: graphitic-N at 401.2 eV, pyrrolic-N at 400.7 eV as well as pyridinic-N at 398.6 eV (Figure 4d). Generally, it has been widely recognized that all the N bonding configurations, except for N-oxide, contribute to the electrocatalytic activity.³⁹⁻⁴⁰ Specifically, the graphitic-N has been proved to afford more valence electrons to enhance the conductivity and electrocatalytic activity.⁴¹⁻⁴² Therefore, we can speculate the origins for the superior electrocatalytic activity of Mn-CoP nanosheets compare with CoP and Mn-CoP nanoparticles. At first, the nanosheets morphology presents larger specific surface area (357.7 m²·g⁻¹) and higher porosity, which could afford more catalytic active sites and promote electrons transfer and masses transport. Second, Mn doping can weaken the adsorption between Co and H atoms, resulting in more thermo-neutral hydrogen adsorption free energy.²⁰ Last, the carbonation process leads to a higher electrical conductivities and active N doping species of Mn-CoP nanosheets.

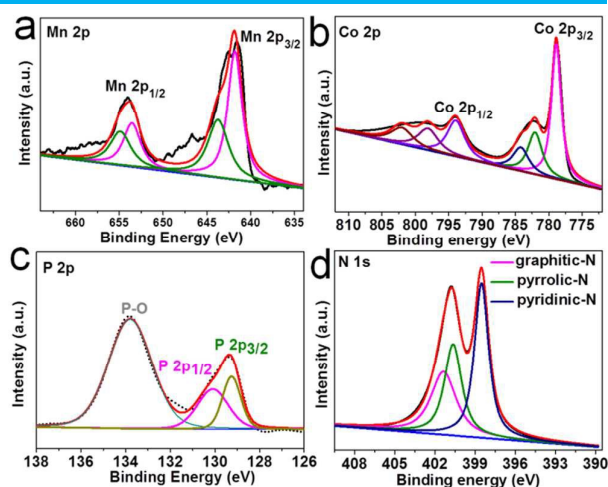


Figure 4 XPS of (a) Mn 2p spectrum; (b) Co 2p spectrum; (c) P 2p spectrum; (d) N 1s spectrum;

Conclusions

ARTICLE

Journal Name

We have elaborately prepared a novel nanocomposite Mn-CoP with 2D structural nanosheets through an etching-carbonization-phosphidation strategy using well-defined rhombic dodecahedral ZIF-67 as a precursor. The Mn-CoP nanosheets catalyst demonstrates superior bifunctional HER and OER electrocatalytic performances in acidic and alkaline system. The required overpotentials are 148 and 195 mV for the HER in acidic 0.5 M H₂SO₄ and alkaline 1 M KOH to acquire the current density of 10 mA·cm⁻², respectively. The catalyst also exhibits outstanding OER performance with the overpotential of 290 mV to achieve 10 mA·cm⁻², comparable with commercial RuO₂. Importantly, the Mn-CoP nanosheets catalyst could maintain remarkable stability for both the HER and OER. The larger BET, hierarchical pore and intrinsic active of Mn-CoP nanosheets accounting for the efficient catalytic performance. Significantly, the optimized electronic structure and adsorption energy after doped Mn and N elements further effectively boosting the electrocatalytic performance. Meanwhile, this work enlightens new design of highly active and stable structured TMPs nanocomposites catalysts for electrocatalysis applications.

Conflicts of interest

There are no conflicts to declare.

Acknowledgements

This work was supported by the Thousand Talents Plan Foundation of China and Guangdong Province, and the 100 Talents Plan Foundation of Sun Yat-sen University (31000-18821107), the Program for Guangdong Introducing Innovative and Entrepreneurial Teams (2017ZT07C069).

Notes and references

- S. Chu and A. Majumdar, *Nature*, 2012, **488**, 294-303.
- L. Han, J. D. jun Dong and E. K. Wang, *Adv. Mater.* 2016, **28**, 9266-9291.
- W. Zhang, W. Lai and R. Cao, *Chem. Rev.*, 2017, **117**, 3717-3797.
- N. Su, Y-J Xu, H. M. Chen. *Chem. Soc. Rev.*, 2017, **46**, 337-365.
- Z. Lu, X. Sun and Y. Cui, *Nat. Commun.* 2014, **5**, 4345.
- Y. Xu, M. Kraft and R. Xu, *Chem. Soc. Rev.*, 2016, **45**, 3039-3052.
- Y. Yan, B. Y. Xia, B. Zhao and X. Wang, *J. Mater. Chem. A*, 2016, **4**, 17587-17603.
- S. Ma, Q. Zhu, L. Chen, W. Wang and D. Chen, *J. Mater. Chem. A*, 2016, **4**, 8149-8154.
- Z. Zhao, H. Wu, H. He, X. Xu and Y. Jin, *J. Mater. Chem. A*, 2015, **3**, 7179-7186.
- S. Ci, S. Mao, Y. Hou, S. Cui, H. Kim, R. Ren, Z. Wen and J. Chen, *J. Mater. Chem. A*, 2015, **3**, 7986-7993.
- K. Xu, P. Chen, X. Li, Y. Tong, H. Ding, X. Wu, W. Chu, Z. Peng, C. Wu and Y. Xie, *J. Am. Chem. Soc.*, 2015, **137**, 4119-4125.
- R. Liu, Y. Wang, D. Liu, Y. Zou and S. Wang, *Adv. Mater.*, 2017, **29**, 1701546.
- P. Xiao, W. Chen, and X. Wang, *Adv. Energy Mater.* 2015, **5**, 1500985.
- Y. Shi and B. Zhang, *Chem. Soc. Rev.*, 2016, **45**, 1529-1541.
- M. Sun, H. Liu, J. Qu, and J. Li, *Adv. Energy Mater.* 2016, **6**, 1600087
- E. J. Popczun, J. R. McKone, C. G. Read, A. J. Biacchi, A. M. Wiltrout, N. S. Lewis and R. E. Schaak, *J. Am. Chem. Soc.*, 2013, **135**, 9267-9270.
- Y. Zheng, Y. Jiao, M. Jaroniec and S. Qiao, *Angew. Chem., Int. Ed.*, 2015, **54**, 52-65.
- T. Liu, D. Liu, F. Qu, D. Wang, L. Zhang, R. Ge, S. Hao, Y. Ma, G. Du, A. M. Asiri, L. Chen and X. Sun, *Adv. Energy Mater.*, 2017, **7**, 1700020.
- Y. Pan, K. Sun, S. Liu, K. Wu, and Y. D. Li, *J. Am. Chem. Soc.* 2018, **140**, 2610-2618.
- D. Li, H. Baydoun, C. N. Verani, and S. L. Brock, *J. Am. Chem. Soc.* 2016, **138**, 4006-4009.
- Y. Li, J. Liu, C. Chen, X. Zhang, and J. Chen, *ACS Appl. Mater. Interfaces* 2017, **9**, 5982-5991.
- R. Zhang, C. Tang, A. M. Asiri, L. Chen and X. Sun, *Nanoscale*, 2017, **9**, 4793-4800.
- T. Liu, X. Ma, D. Liu, S. Hao, G. Du, Y. Ma, A. M. Asiri, X. Sun, and L. Chen, *ACS Catal.* 2017, **7**, 98-102.
- Y. Suna, L. Hang, Q. Shen, T. Zhang, H. Li, X. Zhang, Y. Li, *Nanoscale*, 2017, **9**, 16674-16679.
- X. Xiao, C. He, S. Zhao, J. Li, W. Lin, Z. Yuan, Q. Zhang, S. Wang, L. Dai and D. Yu, *Energy Environ. Sci.*, 2017, **10**, 893-899.
- H. Furukawa, K. E. Cordova, M. O. Keeffe, O. M. Yaghi. *Science*, 2013, **341**, 1230444.
- M. Liu and J. Li, *ACS Appl. Mater. Interfaces* 2016, **8**, 2158-2165.
- L. Jiao, Y. Zhou and H. Jiang, *Chem. Sci.*, 2016, **7**, 1690-1695.
- Z. Zhang, J. Hao, W. Yang, and J. Tang. *ChemCatChem*, 2015, **7**, 1920-1925.
- X. Li, Q. Jiang, S. Dou, L. Deng, J. Huo and S. Wang. *J. Mater. Chem. A*, 2016, **4**, 15836-15840.
- R. Wu, D. P. Wang, K. Zhou, N. Srikanth, J. Wei and Z. Chen. *J. Mater. Chem. A*, 2016, **4**, 13742-13745.
- M. Xu, L. Han, Y. Han, Y. Yu, J. Zhai and S. Dong. *J. Mater. Chem. A*, 2015, **3**, 21471-21477.
- J. Ping, H. Zhang, *Adv. Mater.* 2016, **28**, 7640-7645.
- X. Long, J. Li, S. Xiao, K. Yan, Z. Wang, H. Chen, S. Yang, *Angew. Chem. Int. Ed.* 2014, **53**, 7584-7588.
- S. Chen, J. Duan, M. Jaroniec and S. Qiao, *Angew. Chem., Int. Ed.*, 2013, **52**, 13567-13570.
- L. Xiao, S. Zhang, J. Pan, C. Yang, M. He, L. Zhuang and J. Lu, *Energy Environ. Sci.*, 2012, **5**, 7869-7871.
- J. R. McKone, B. F. Sadtler, C. A. Werlang, N. S. Lewis and H. B. Gray, *ACS Catal.*, 2013, **3**, 166-169.
- E. J. Popczun, J. R. McKone, C. G. Read, A. J. Biacchi, A. M. Wiltrout, N. S. Lewis and R. E. Schaak, *J. Am. Chem. Soc.*, 2013, **135**, 9267-9270.
- S. Fu, C. Zhu, J. Song, D. Du, Y. Lin, *Adv. Energy Mater.* 2017, **7**, 1700363.
- J. Liu, D. Zhu, C. Guo, A. Vasileff, and S. Qiao, *Adv. Energy Mater.* 2017, **7**, 1700518.
- D. H. Guo, R. Shibuya, C. Akiba, S. Saji, T. Kondo and J.

Journal Name

ARTICLE

- Nakamura, *Science*, 2016, **351**, 361-365.
42. W. J. Lee, U. N. Maiti, J. M. Lee, J. Lim, T. H. Han and S. O. Kim, *Chem. Commun.*, 2014, **50**, 6818-6930.